



HAL
open science

Mathematical investigation of innate immune responses to lung cancer: The role of macrophages with mixed phenotypes

Raluca Eftimie, Charlotte Barelle

► **To cite this version:**

Raluca Eftimie, Charlotte Barelle. Mathematical investigation of innate immune responses to lung cancer: The role of macrophages with mixed phenotypes. *Journal of Theoretical Biology*, 2021, 524, pp.110739. 10.1016/j.jtbi.2021.110739 . hal-03258055

HAL Id: hal-03258055

<https://hal.science/hal-03258055>

Submitted on 11 Jun 2021

HAL is a multi-disciplinary open access archive for the deposit and dissemination of scientific research documents, whether they are published or not. The documents may come from teaching and research institutions in France or abroad, or from public or private research centers.

L'archive ouverte pluridisciplinaire **HAL**, est destinée au dépôt et à la diffusion de documents scientifiques de niveau recherche, publiés ou non, émanant des établissements d'enseignement et de recherche français ou étrangers, des laboratoires publics ou privés.

Mathematical investigation of innate immune responses to lung cancer: the role of macrophages with mixed phenotypes

Raluca Eftimie^{a,b,*}, Charlotte Barelle^a

^a*Division of Mathematics, University of Dundee, Dundee, United Kingdom, DD1 4HN*

^b*Laboratoire Mathématiques de Besançon, UMR - CNRS 6623, Université de Bourgogne Franche-Comté, 25000 Besançon, France*

Abstract

Macrophages' role in the evolution of solid tumours is a well accepted fact, with the M1-like macrophages having an anti-tumour role and the M2-like macrophages having a pro-tumour role. Despite the fact that some clinical studies on lung tumours have emphasised also the presence of macrophages with mixed M1 and M2 phenotypes in addition to macrophages with distinct phenotypes, the majority of studies still use the distinct M1-M2 classification to predict the evolution of tumours and patient survival. In this theoretical study we use a mathematical modelling and computational approach to investigate the role of macrophages with mixed phenotype on growth/control/elimination of lung tumours. We show that tumour control in the presence of M2→M1 re-polarising treatments is mainly the result of macrophages with mixed phenotypes (due to the assumption of short half-life of M1-like macrophages). We also show that the half-life of various macrophage phenotypes (distinct M1 or mixed M1/M2 phenotypes) impacts the outcome of various therapeutic strategies targeting tumour-associated macrophages. All these results suggest the need for a better experimental understanding of the kinetics of macrophages inside solid tumours.

Keywords: Mathematical modelling; Non-small cell lung cancer; M1 and M2 macrophages; Macrophages with mixed phenotypes;

2020 MSC: 92C50

1. Introduction

2 The non-small cell lung cancer is the most common type of lung cancers,
3 and the leading cause of cancer-related deaths in the world [1, 2]. Due to the

*Corresponding author

Email address: r.a.eftimie@dundee.ac.uk; raluca.eftimie@univ-fcomte.fr (Raluca Eftimie)

4 absence of clinical symptoms, most cancers are diagnosed only when they reach
5 an advanced stage and when treatments are not effective anymore. For a long
6 time it was thought that NSCLC is non-immunogenic, but over the last decade a
7 number of studies have shown that this lack of immunity is the result of immune-
8 evasive mechanisms employed by the tumour cells [1]. A recent study [3] on the
9 immune cell composition of human NSCLC has shown that T cells represent the
10 most abundant immune cell population ($\approx 47\%$), followed by B cells ($\approx 16\%$),
11 macrophages ($\approx 4.7\%$) and NK cells ($\approx 4.5\%$). However, in [4] the authors
12 found that neutrophils are the most prevalent immune cells in NSCLC, while
13 in [5] the authors identified more macrophages than T cells inside tumour islets
14 and stroma. A very recent study [6] that analysed publicly available raw mi-
15 croarray expression data on immune composition of NSCLC concluded that the
16 majority of the immune infiltrates inside these tumours is represented by the
17 macrophages, followed by T cells and B cells. Moreover, in regard to the in-
18 filtrating macrophages, the authors in [6] concluded that the majority of these
19 cells have a M2-like phenotype (i.e., alternatively activated, anti-inflammatory
20 and pro-tumour cells [7]), with the next abundant cells having M1-like pheno-
21 types (i.e., classically activated, pro-inflammatory and anti-tumour cells [7]) or
22 M0 (non-activated) phenotypes. It is possible that some of these contradictory
23 results might be the result of the type of cell markers used to classify the cells,
24 including the different types of macrophages, as discussed below in more detail.

25 Because many clinical studies [8, 9, 10, 11, 12] have focused on the prognos-
26 tic value of the numbers/percentages of various macrophage sub-populations
27 that infiltrate various tumour areas (islets, stroma) in NSCLC patients, in this
28 study we focus on the role of macrophages on the growth, control, and elim-
29 ination of lung tumours. Again, we need to emphasise that all these clinical
30 studies on NSCLC show different results, some being reproduced and sum-
31 marised in Figure 1. One reason for these differences could be the various
32 markers used to classify the various cell types; e.g., CD68/iNOS [9, 11] and
33 CD68/HLA-DR [8, 9] for M1 cells; CD68/CD163 [8, 9, 11], CD68/CD204 [12],
34 CD68/CD206 [13] for M2 cells). In addition, a number of studies that profiled
35 human NSCLC showed that a small percentage of macrophages (i.e., between
36 0-11%) have markers characterising M2 cells as well as markers characterising
37 M1 cells [8, 9, 12]; see also Figure 1(a),(b). However, in a very recent study [14]
38 on early-stage lung cancer the authors showed experimentally that tumour-
39 associated macrophages from NSCLC expressed both M1 and M2 markers (e.g.
40 HLA-DR, CD206, CD163), sometimes at levels higher than the *in vitro* differ-
41 entiated M1 and M2 macrophages. They also showed that approximately 40%
42 of CD14⁺ cells identified inside the NSCLC tissue had high levels of both HLA-
43 DR and CD163 markers, and more than 50% had high levels of both HLA-DR
44 and CD206 markers. (Note that CD14⁺ is a human protein produced mostly by
45 macrophages.) Returning to Figure 1, we also note that since some of the mark-
46 ers can be expressed by both M1 and M2 cells, the percentages shown in some
47 of the sub-panels, e.g., sub-panel (b), do not add up to 100%. We can conclude
48 from here that there are still many contradictory results about the proportion
49 of macrophages with mixed phenotypes inside lung tumours (probably due to

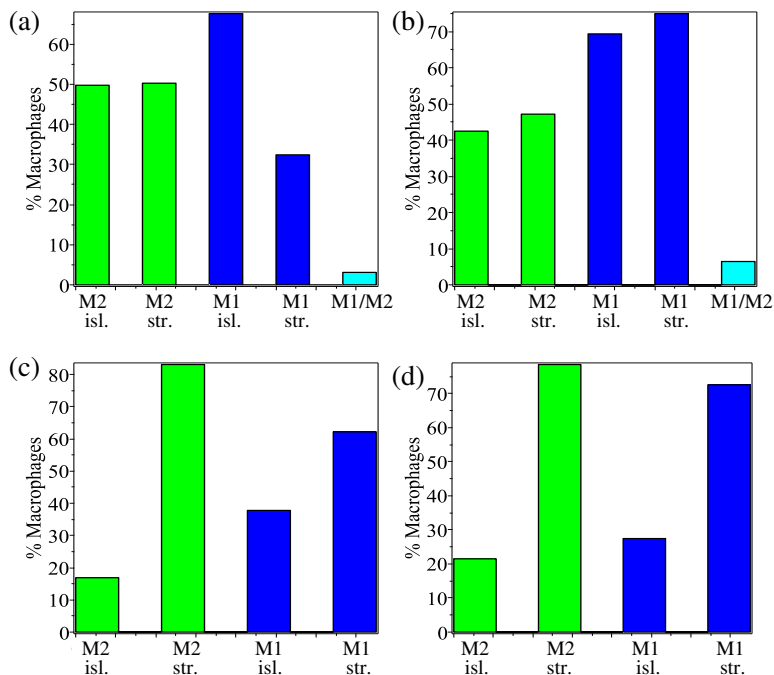


Figure 1: Data on macrophage percentages in tumour islets (isl.) and stroma (str.) as we approximated it from the following clinical studies on NSCLC: (a) the study in [8]. Here we show data for M1 (blue) and M2 (green) percentages in long-term patients survival - to compare it with the study in [9]. Percentages were calculated using the data from Table 2 in [8], by taking the ratio of M1 (or M2) cell numbers in either islets or stroma to the total number of M1 (or M2) cells inside both islets and stroma. The authors also mentioned the existence of a small percentage of cells with mixed M1/M2 phenotype (between 1.2%-8.1% with a median of 3.1%; see the cyan-coloured bar). (b) the study in [9]. Here we show data for long-term patients survival. Percentages were taken directly from Table 2 in [9]. The authors also mentioned the existence of a small percentage of cells with mixed M1/M2 phenotype (between 2.5%-10.2% with a median of 6.45%; see the cyan-coloured bar). (c) the study in [10], where there was no mention on whether the data was for long-term or short-term patients. Percentages were taken directly from Table 2 in [10]; (d) the study in [11], where again there was no mention on whether the data was for long-term or short-term patients. We calculated the percentages using the data from Table 3 in [11], by taking the ratio of the total number of M1 (or M2) cells (from patients with stage IIA-IIB cancers) in either islets or stroma over the total number of M1 (or M2) cells inside both islets and stroma. Similar results were obtained for macrophage data from patients with stage IA-IB or IIIA-IIIB cancers.

50 the fact that the classification of macrophages subsets is still in its infancy [15]
 51 and still poses many challenges [16]).

52 To address various questions related to tumour-macrophage interactions (as
 53 well as questions about the effect of different immuno- and chemo-therapies on
 54 tumour-macrophage interactions), the last few decades have seen the develop-
 55 ment of a large variety of mathematical models [17, 18, 19, 20, 21, 22, 23, 24].
 56 We note that all these models focus on the two extreme types of macrophages,

57 M1-like and M2-like cells, and ignore the possible role of macrophages with
58 mixed phenotypes.

59 In this paper we use a mathematical modelling and computational approach
60 to shed some light on the following questions:

- 61 • What biological mechanisms influence the level of macrophages with mixed
62 M1/M2 phenotypes?
- 63 • What is the importance of macrophages with mixed M1/M2 phenotypes
64 on tumour growth/control/elimination?

65 To this end, we derive a new mathematical model (an extension of a simple
66 model introduced in [20]) that considers the interactions between a homoge-
67 neous NSCLC population and three macrophage sub-populations: the M1 cells,
68 the M2 cells, and cells with mixed M1/M2 phenotypes. Despite the human
69 macrophage data shown in Figure 1, there are very little other human studies
70 that would allow us to obtain a better understanding of the mechanisms in-
71 volved in the macrophage-tumour interactions in human lungs. For this reason,
72 in this study we focus on murine data to parametrise this new mathemati-
73 cal model for tumour-macrophage interactions. Numerical simulations are per-
74 formed to understand the role of macrophage polarisation rates ($M1 \rightarrow M2$) and
75 re-polarisation rates ($M2 \rightarrow M1$) on the reduction/growth in tumour size, as well
76 as the interactions between these rates and cell kinetics on tumour evolution.

77 The paper is structured as follows: in Section 2 we introduce the new math-
78 ematical model and parametrise it with murine data; in Section 3 we discuss
79 the dynamics of this new model as we vary the initial conditions and different
80 model parameters. Due to the uncertainty in the parameter values, we also per-
81 form local and global sensitivity analysis to shed some light on the important
82 parameters. We conclude in Section 4 with a summary and discussion of the
83 results.

84 2. Model Description

The following mathematical model is used to describe and investigate the interactions between tumour cells and macrophages. This model focuses on the temporal evolution of: tumour cells (u_T), macrophages with a M1-like phenotype (u_{M1}), macrophages with a M2-like phenotype (u_{M2}), and macrophages

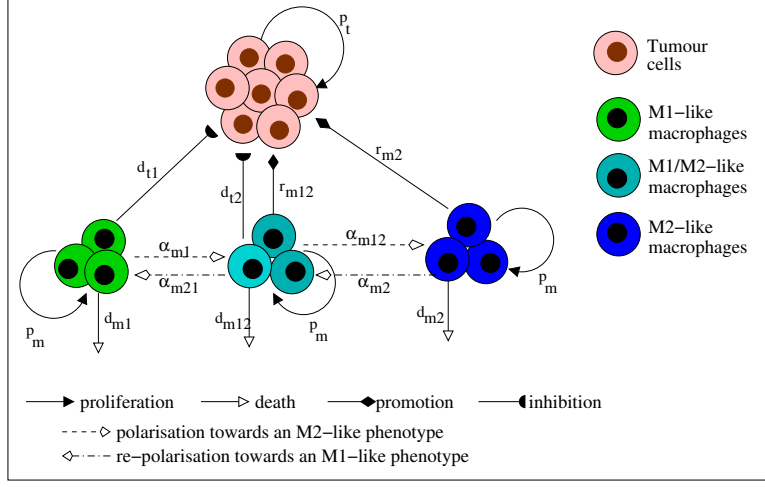


Figure 2: Caricature description of the cell-cell interactions depicted by model (1).

with a mixed M1-M2 phenotype (u_{M12}); see also Figure 2.

$$\frac{du_T}{dt} = p_t u_T \left(1 - \frac{u_T}{K_t}\right) (1 + r_{m2} u_{M2} + r_{m12} u_{M12}) - d_{t1} u_T u_{M1} - d_{t2} u_T u_{M12}, \quad (1a)$$

$$\begin{aligned} \frac{du_{M1}}{dt} = & p_{m1} u_{M1} \left(1 - \frac{u_{M1} + u_{M12} + u_{M2}}{K_m}\right) - d_{m1} u_{M1} - \alpha_{m1} u_{M1} \frac{u_T}{u_T + K_t^*} \\ & + \alpha_{m21} u_{M12}, \end{aligned} \quad (1b)$$

$$\begin{aligned} \frac{du_{M12}}{dt} = & p_{m12} u_{M12} \left(1 - \frac{u_{M1} + u_{M12} + u_{M2}}{K_m}\right) - d_{m12} u_{M12} + \alpha_{m1} u_{M1} \frac{u_T}{u_T + K_t^*} \\ & - \alpha_{m12} u_{M12} \frac{u_T}{u_T + K_t^*} - \alpha_{m21} u_{M12} + \alpha_{m2} u_{M2}, \end{aligned} \quad (1c)$$

$$\begin{aligned} \frac{du_{M2}}{dt} = & p_{m2} u_{M2} \left(1 - \frac{u_{M1} + u_{M12} + u_{M2}}{K_m}\right) - d_{m2} u_{M2} + \alpha_{m12} u_{M12} \frac{u_T}{u_T + K_t^*} \\ & - \alpha_{m2} u_{M2}. \end{aligned} \quad (1d)$$

85 The above equations incorporate the following biological assumptions:

- 86 • Equation (1a) describes the dynamics of tumour cells, which are assumed
87 to grow logistically at a rate p_t up to a carrying capacity K_T . This
88 logistic growth models the phenomenological observation that tumour
89 growth slows down as size increases, due to lack of nutrients [25]. The
90 macrophages with a M2-like phenotype (u_{M2} and u_{M12}) contribute to the
91 proliferation of tumour cells [26, 7, 16], which we model using coefficients
92 r_{m2} and r_{m12} . The macrophages with a M1-like phenotype reduce tumour
93 growth [7] at rates d_{t1} (the u_{M1} cells) and d_{t2} (the u_{M12} cells).

- 94 • Equation (1b) describes the dynamics of macrophages with a dominant
95 M1 phenotype (u_{M1}). Since tissue-resident macrophages are maintained
96 via self-proliferation with minimal monocyte input [27, 28, 29], and since
97 in [30] the authors showed that macrophages have an exponential growth
98 followed by a stationary phase, here we consider a logistic growth at a
99 rate p_{m1} , up to a carrying capacity K_m . These cells die naturally [31]
100 at a rate d_{m1} . In the presence of tumour cells, the M1 macrophages can
101 polarise (at a rate α_{m1}) towards a mixed M1/M2 phenotype. External
102 factors (e.g., anti-tumour treatments [32]) can re-polarise (at a rate α_{m21})
103 the macrophages with a mixed M1/M2 phenotype towards an anti-tumour
104 M1-dominant phenotype.
- 105 • Equation (1c) describes the dynamics of macrophages with mixed M1/M2
106 phenotype (u_{M12}). As before, since tissue-resident macrophages are self-
107 proliferating [27, 28] and their proliferation has an exponential phase fol-
108 lowed by a stationary phase [30], here we assume a logistic growth at a rate
109 p_{m12} , up to a carrying capacity K_m . Moreover, these cells die naturally
110 at a rate d_{m12} . Finally, we assume that these cells with mixed M1/M2
111 phenotypes can polarise (at a rate α_{m12}) in the presence of tumour cells
112 towards a more distinct M2 phenotype, or can re-polarise (at a rate α_{m21})
113 following external treatment [32] towards an M1 phenotype. In the pres-
114 ence of tumour cells, M1 macrophages can polarise (at a rate α_{m1}) towards
115 a mixed M1/M2 phenotype. Anti-tumour treatments [32] can re-polarise
116 (at a rate α_{m2}) the M2 macrophages towards a mixed M1/M2 phenotype.
- 117 • Equation (1d) describes the dynamics of macrophages with a dominant
118 M2 phenotype (u_{M2}). Again, we assume that this population grows lo-
119 gistically at a rate p_{m2} , up to a carrying capacity K_m . These cells die
120 naturally at a rate d_{m2} [31]. Anti-tumour treatments [32] can re-polarise
121 the M2 macrophages (at a rate α_{m2}) towards a mixed M1/M2 phenotype.
122 In the presence of tumour cells, the macrophages with a mixed M1/M2
123 phenotype can polarise (at a rate α_{m12}) towards M2 cells.

124 2.1. Parameter estimation

125 Even if our biological questions were triggered by human NSCLC data (see
126 Figure 1), to identify some of the model parameters we focus on murine experi-
127 ments for which there is more data (compared to humans). Below we summarise
128 the data we used to estimate different model parameters.

- 129 • The study in [33] investigated the growth of tumours resembling non-
130 small cell lung cancer (NSCLC) in mice lungs. In Figure 3 we reproduce
131 the murine tumour growth data from [33], together with the solution of a
132 logistic equation for tumour growth. The best fit of the numerical solution
133 to the data (obtained using the classical least square method) was obtained
134 for $p_t = 0.23$ and $K_t = 1400$. This proliferation rate is consistent with the
135 doubling time (i.e., 2.97 days) of NSCLC cells inoculated into nude mice,
136 as calculated experimentally in [34].

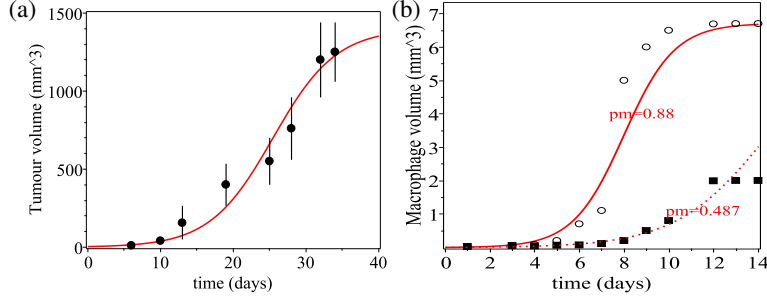


Figure 3: (a) Reproduction of tumour growth data from [33] (black circles) together with the solution of a logistic growth equation for tumour growth (red curve), as given by eq. (1a) in the absence of any macrophages. Here $K_t = 1400$ and $p_t = 0.23$, and the initial condition for the numerical simulation of the tumour logistic growth is $u_T(0) = 4\text{mm}^3$. (b) Reproduction of macrophage growth data from [30] (open circles and black squares) – where data was transformed from number of cells to potential volume occupied by these cells (see discussion below) – together with the solution of a logistic equation for macrophage growth (red curves), as given by the sums of eqs. (1b)+(1c)+(1d) when $p_{m1} = p_{m12} = p_{m2} := p_m$ and $d_{m1} = d_{m12} = d_{m2} = 0$. The continuous curve was obtained for $p_m = 0.88$ and $K_m = 6.72$, while the dotted curve was obtained for $p_m = 0.483$ and $K_m = 6.72$. The initial condition for the numerical simulation of macrophage logistic equation is $u_M(0) = 0.006\text{mm}^3$ (where u_M describes the total macrophage size).

- 137 • In [3] the authors have calculated that macrophages represent $\approx 4.8\%$ of
138 the total immune infiltrates into human NSCLC. For our murine model,
139 we assume that immune cell infiltrates represent up to 10% of tumour
140 mass, and the macrophages represent 4.8% of these immune infiltrates.
141 (Note that in [10] it was estimated that macrophages represent $\approx 15.84\%$
142 of all cells inside tumour tissue, and thus our assumption is not completely
143 unrealistic.) Thus, for a maximum tumour volume of $K_t = 1400\text{mm}^3$ we
144 obtain a maximum macrophage volume of $K_m = 6.72\text{mm}^3$.
- 145 • In [35] the authors calculated the diameter of an alveolar macrophage at
146 $\approx 19\mu\text{m}$. In [36] the author suggested that a volume of 1000mm^3 can
147 contain up to 9.39×10^7 cells of diameter $22\mu\text{m}$, or up to 2.44×10^8 cells of
148 diameter $16\mu\text{m}$. In this study, we assume that a volume of 1000mm^3 can
149 contain $\approx 10^8$ macrophages. Thus a carrying capacity $K_m = 6.72\text{mm}^3$
150 can contain $\approx 6.72 \times 10^5$ macrophages. These numbers are consistent
151 with the experimental study in [37], where the authors showed that the
152 number of macrophages from control mice ranged from 8×10^4 cells/mouse
153 to 2.4×10^5 cells/mice.
154 In [30], the authors measured macrophage growth, and calculated a pro-
155 liferation rate between 0.487/day and 0.88/day (in different mice). In
156 Figure 3 we approximated the two macrophage data sets from [30] (Fig.
157 14.20.1 in [30], which shows cell numbers), where we transformed cell num-
158 bers into cell volumes (using the assumptions and calculations above).
159 Since in [30] the authors showed that macrophages grow logistically, we

160 fitted a logistic growth curve with rate p_m and carrying capacity $K_m =$
 161 6.72mm^3 . The continuous red curve in Figure 3 shows macrophage growth
 162 for $p_m = 0.88$, while the dashed red curve shows macrophage growth
 163 for $p_m = 0.487$. Throughout this study we will consider an average
 164 macrophage proliferation rate of $p_{m1} = p_{m12} = p_{m2} = 0.7$.

165 • The experimental study in [27], which focused on the adoptive trans-
 166 fer of human mononuclear phagocytes into mice, showed that classical
 167 (M1) macrophages circulate for a mean of 1.01 days, whereas intermedi-
 168 ate (M12) and nonclassical (M2) macrophages have longer mean lifespans
 169 of 4.30 and 7.41 days, respectively. In [31] the authors stated that the
 170 murine M1-like macrophages (involved in phagocytosis) have a half-life
 171 between 18-20hrs, while the murine M2-like macrophages (involved in tis-
 172 sue repair) have a half-life between 5-7 days. Therefore, in this study we
 173 assume that:

- 174 – the M1-like macrophages have a half-life of ≈ 0.8 days (i.e., $\approx 19.2\text{hr}$),
 175 corresponding to a death rate $d_{m1} = 0.87/\text{day}$;
- 176 – the mixed M1/M2 macrophages have a half-life of ≈ 3 days, corre-
 177 sponding to a death rate $d_{m12} = 0.23/\text{day}$;
- 178 – the M2-like macrophages have a half-life of ≈ 5.14 days, correspond-
 179 ing to a death rate $d_{m2} = 0.09/\text{day}$.

180 All other parameter values that appear in model (1) are unknown. In the
 181 following, we discuss some of the assumptions we consider when choosing the
 182 ranges over which we vary these parameters:

- 183 • We assume that the presence of 1% of max tumour is enough to trigger a
 184 $u_{M1} \rightarrow u_{M12}$ polarisation, and further a $u_{M12} \rightarrow u_{M2}$ polarisation. Thus,
 185 we consider $K_t^* = 1\%K_t$.
- 186 • We assume that macrophages with mixed M1/M2 phenotypes exhibit half
 187 the anti-tumour effect of the M1 macrophages. Thus, we consider $d_{t1} \in$
 188 $(10^{-5}, 10^{-1})$ (with a baseline value of $d_{t1} = 0.01$) and $d_{t2} \in (5 \times 10^{-6}, 5 \times$
 189 $10^{-2})$ (with a baseline value of $d_{t2} = 0.005$).
- 190 • We assume that macrophages with mixed M1/M2 phenotype have half the
 191 pro-tumour effect of M2 macrophages. Thus, we consider $r_{m2} \in (10^{-2} -$
 192 $10^0)$ (with a baseline value $r_{m2} = 0.1$) and $r_{m12} \in (5 \times 10^{-3}, 0.5)$ (with a
 193 baseline value $r_{m12} = 0.05$).
- 194 • In humanised murine experiments [27] it has been found that that only
 195 a small proportion of M1 macrophages will re-polarise to an intermedi-
 196 ate M12 phenotype, but most M12 macrophages will re-polarise to an
 197 M2 phenotype during their lifespan. Throughout this study we assume
 198 $\alpha_{m1} < \alpha_{m12}$. For the re-polarisation rates we assume $\alpha_{m2} = \alpha_{m21}$. Thus,
 199 we consider $\alpha_{m1} \in (10^{-4}, 10^{-1})/\text{day}$ (with a baseline $\alpha_{m1} = 10^{-3}/\text{day}$),
 200 $\alpha_{m12} \in (10^{-3}, 10^{-1})/\text{day}$ (with a baseline of $\alpha_{m12} = 10^{-2}/\text{day}$), and

201 $\alpha_{m2} = \alpha_{m21} \in (10^{-3}, 10^0)/\text{day}$ (with baselines of 0.0, since we assume
 202 that initially there is no treatment to force a macrophage re-polarisation
 203 towards an M1-like phenotype).

204 All these estimated parameter values and ranges which appear in model (1)
 205 are summarised in Table 2.1. For simplicity, and to avoid numerical problems
 206 caused by a stiff system, we rescale the tumour cells by K_t and the macrophages
 207 by K_m . This leads to unitary carrying capacities ($\overline{K}_t = 1, \overline{K}_m = 1$), and to a
 208 rescaling of the following five parameters:

$$\begin{aligned} \overline{d_{t1}} &= d_{t1} \times K_m, & \overline{d_{t2}} &= d_{t2} \times K_m, & \overline{r_{m2}} &= r_{m2} \times K_m, \\ \overline{r_{m12}} &= r_{m12} \times K_m, & \overline{K_t^*} &= \frac{K_t^*}{K_t}. \end{aligned} \quad (2)$$

209 These rescaled parameter values are listed in the fourth column in Table 2.1
 210 – where we removed the bars for simplicity. These values are used for the
 211 numerical simulations performed throughout this study.

212 3. Numerical results

213 The initial conditions for the numerical simulations of system (1) were ob-
 214 tained from the rescaled initial conditions in Figure 3:

$$\begin{aligned} u_T(0) &= \frac{4}{K_t} = \frac{4}{1400} = 0.002857, \\ u_{M1}(0) &= \frac{0.006}{K_m} = \frac{0.006}{6.72} = 0.000893, \\ u_{M12}(0) &= 0.0, \quad u_{M2}(0) = 0.0. \end{aligned} \quad (3)$$

215 Thus, we assume that when the tumour is introduced into the system, it elicits
 216 a pro-inflammatory immune response characterised only by the presence of a
 217 non-zero u_{M1} population. The numerical solution is propagated in time using
 218 a classical fourth order Runge-Kutta method.

219 3.1. Baseline system dynamics

220 Figure 4(a) shows the dynamics of model (1) for the baseline parameter
 221 values given in Table 2.1. We see that initially ($t < 10$ days) the immune
 222 response is dominated by macrophages with a M1 phenotype. Then a transient
 223 increase in the cells with a mixed M1/M2 phenotype (for $10 < t < 30$) is
 224 associated with a reduction in tumour size. Tumour relapse is associated with
 225 an increase in the cells with a M2 phenotype (for $t > 40$). We emphasise here
 226 that this baseline case assumes $\alpha_{m2} = \alpha_{m21} = 0$ (see Table 2.1), i.e., no external
 227 immune treatment to induce a re-polarisation of M2-like macrophages towards
 228 an M1-like phenotype [32].

229 In Figure 4(b) we show the effect of externally-inducing a macrophage re-
 230 polarisation on model (1); i.e., $\alpha_{m2} = \alpha_{m21} = 0.01$. We observe a slight reduc-
 231 tion in tumour size in the long term (i.e. $t > 80$ days), which is associated with

Table 1: Summary of the parameter values used in this study. The 2nd column shows the dimensional parameters, the 3rd column shows their units, and the 4th column shows in bold the rescaled parameter values; see eq. (2) (If there is no difference between the values in the 2nd and 4rd column, it means that the parameter was not rescaled). For most of the parameter values we show a whole range, with the value inside the parentheses being the baseline value used for the simulations. The time unit is “day”, cells are described by cell volume “vol”.

Param.	Original values	Original Units	Rescaled values	Description (original values)
p_t	0.23	$\frac{1}{day}$	0.23	Proliferation rate of tumour cells
K_t	1400	vol	1	Tumour carrying capacity
K_t^*	14	vol	0.01	Tumour level that triggers M1→M2 macrophage polarisation
r_{m2}	$10^{-2} - 10^0$ (0.1)	$\frac{1}{vol}$	6.72×10^{-2} – 6.72 (0.672)	Contribution of M2 macrophages to the proliferation of tumour cells
r_{m12}	$0.005 - 0.5$ (0.05)	$\frac{1}{vol}$	0.0336 – 3.36 (0.336)	Contribution of macrophages with mixed M1/M2 phenotype to the proliferation of tumour cells
d_{t1}	$10^{-2} - 10^0$ (0.2)	$\frac{1}{day \cdot vol}$	6.72×10^{-2} – 6.72 (1.344)	Tumour killing rate by M1 macrophages
d_{t2}	$5 \times 10^{-3} - 0.5$ (0.1)	$\frac{1}{day \cdot vol}$	3.36×10^{-2} – 3.36 (0.672)	Tumour killing rate by macrophages with mixed M1/M2 phenotype
p_{m1}	$0.487 - 0.88$ (0.7)	$\frac{1}{day}$	$0.487 - 0.88$ (0.7)	Proliferation rate of M1 cells
p_{m12}	$0.487 - 0.88$ (0.7)	$\frac{1}{day}$	$0.487 - 0.88$ (0.7)	Proliferation rate of macrophages with mixed M1/M2 phenotype
p_{m2}	$0.487 - 0.88$ (0.7)	$\frac{1}{day}$	$0.487 - 0.88$ (0.7)	Proliferation rate of M2 cells
K_m	6.72	vol	1	Macrophages carrying capacity
d_{m1}	$0.83-0.924$ (0.87)	$\frac{1}{day}$	$0.83 - 0.924$ (0.87)	Natural death rate of M1 cells
d_{m12}	$0.14-0.83$ (0.23)	$\frac{1}{day}$	$0.14 - 0.83$ (0.23)	Natural death rate of cells with mixed M1/M2 phenotype
d_{m2}	$0.09-0.14$ (0.1)	$\frac{1}{day}$	$0.09 - 0.14$ (0.1)	Natural death rate of M2 cells
α_{m1}	$10^{-5} - 10^{-2}$ (0.001)	$\frac{1}{day}$	$10^{-5} - 10^{-2}$ (0.001)	Polarisation rate of M1 cells towards a mixed M1/M2-phenotype
α_{m12}	$10^{-4} - 10^{-1}$ (0.01)	$\frac{1}{day}$	$10^{-4} - 10^{-1}$ (0.01)	Polarisation rate of macrophages with a mixed M1/M2 phenotype towards a M2-dominant phenotype
α_{m2}	$0 - 10^0$ (0.0)	$\frac{1}{day}$	$0 - 10^0$ (0.0)	Re-polarisation rate of M2 cells towards a mixed M1/M2-phenotype
α_{m21}	$0 - 10^0$ (0.0)	$\frac{1}{day}$	$0 - 10^0$ (0.0)	Re-polarisation rate of macrophages with a mixed M1/M2 phenotype towards a M1-dominant phenotype

232 a higher percentage of macrophages with mixed M1/M2 phenotype (and a very
 233 small but non-zero population of M1-like macrophages). The effect of further
 234 increasing $\alpha_{m2}, \alpha_{m21}$ will be discussed below, in Figure 7(d).

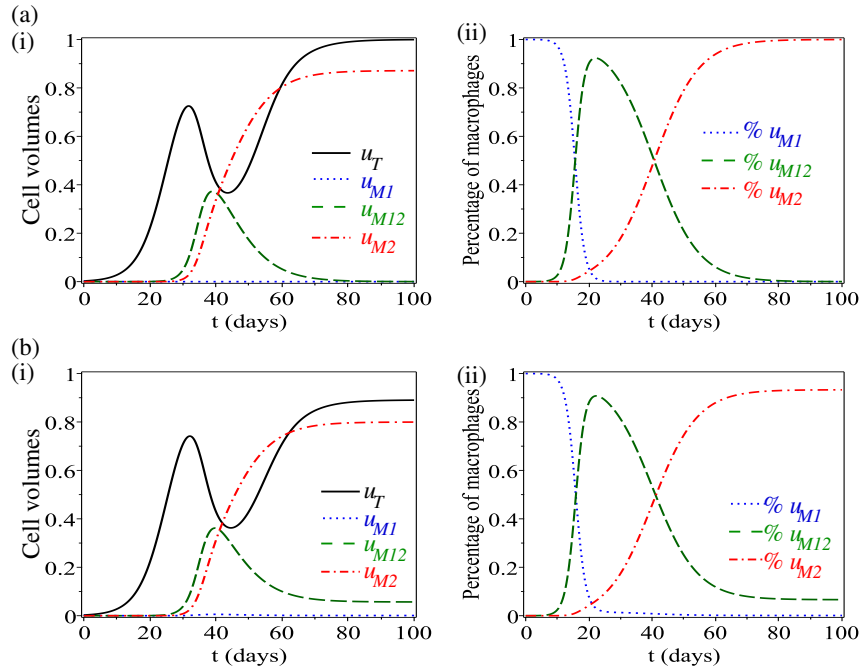


Figure 4: (a) Dynamics of model (1), for the baseline parameter values listed in Table 2.1, when $\alpha_{m2} = \alpha_{m21} = 0$. (b) Dynamics of model (1), when we assume $\alpha_{m2} = \alpha_{m21} = 0.01 > 0$. Sub-panels (i) show the time-evolution of the tumour cells and macrophages; Sub-panels (ii) show the time-evolution of the percentage of macrophage composition.

235 3.2. Sensitivity analysis

236 Since many parameter values were estimated within certain ranges, in the
 237 following we evaluate the robustness of model (1), by investigating the sensi-
 238 tivity of tumour size to small perturbations in some model parameters and in
 239 initial conditions. We start in Section 3.2.1 with a local sensitivity analysis to
 240 investigate how small perturbations in the initial conditions and macrophage
 241 polarisation/re-polarisation rates impact tumour dynamics. However, since we
 242 do not know if there is interaction between these polarisation/re-polarisation
 243 rates and all other estimated parameters that appear in the model, in Sec-
 244 tion 3.2.2, we perform a global sensitivity analysis.

245 3.2.1. Local sensitivity analysis

246 In the following we focus on tumour size at $t = 40$ (while tumour is decreasing
 247 following an increase in macrophages with mixed phenotypes; see Figure 4) and

248 at $t = 60$ (while tumour relapses and is close to its carrying capacity; see
 249 Figure 4). The change in tumour size is calculated using the discrete formula
 250 for the derivative of the output (tumour size) with respect to the input (e.g.,
 251 initial condition $u_j(0)$, where $j \in \{T, M1, M12, M2\}$) [38]:

$$L_S = \frac{u_T^{new}(40) - u_T^{baseline}(40)}{|u_j^{new}(0) - u_j^{baseline}(0)|}. \quad (4)$$

252

253 **Remark 1.** *We decided to focus on time $t = 60$, when the relapsing tumour*
 254 *would approach the carrying capacity (for the baseline parameter values) since*
 255 *we would like to understand the mechanisms that could impact the late-stage*
 256 *tumours, as many lung tumours are discovered when they have already reached*
 257 *a late stage. Moreover, for this local sensitivity analysis we decided to ignore*
 258 *the earlier times (e.g., $t < 30$) since the immune response was too weak at*
 259 *these times, and changes in immune-related parameters had almost no impact*
 260 *on tumour size. We chose to focus on $t = 40$ because at this time the level of*
 261 *immune response (and in particular the macrophages with mixed phenotype) is*
 262 *high enough to have a significant impact on tumour.*

263 **Remark 2.** *In eq. (4) we do not normalise the sensitivity index [39]. This*
 264 *is mainly because when we investigate local sensitivity to the initial conditions,*
 265 *there are two zero baseline initial conditions for u_{M2} and u_{M12} and therefore*
 266 *we cannot divide by these values for normalisation (i.e., the ratio $|u_j^{new}(0) -$*
 267 *$u_j^{baseline}(0)|/u_j^{baseline}(0)$, $j \in \{M12, M2\}$, does not make sense). A similar*
 268 *problem is encountered when we perform the sensitivity to α_{m2} and α_{m21} (which*
 269 *have zero baseline values; see Table 2.1). For this reason, in this study we*
 270 *decided to work with equation (4) and not with a normalised version of this*
 271 *equation.*

272 *Tumour sensitivity to initial conditions.* In Figure 5 we show the magnitude
 273 of changes (i.e., L_S given by eq. (4)) in tumour size on days (a) $t = 40$ and
 274 (b) $t = 60$, as we increase/decrease the initial conditions for the tumour and
 275 M1 macrophage populations by a factor of 10^2 from their baseline values. The
 276 M12 and M2 initial macrophage levels are increased from 0 to 10^{-3} . We see in
 277 Figure 5 that the initial conditions for all macrophage sub-populations have a
 278 significant impact on the early stages of tumour growth (i.e., $t < 50$), and only
 279 the mixed phenotype macrophages seem to play an important role also in the
 280 later stages ($t > 50$). Moreover, increasing the initial tumour size by a factor
 281 of 10^2 does not seem to have an impact on either early or later tumour stages,
 282 which suggests that the baseline initial tumour size is already large enough.
 283 Only a decrease in the initial tumour size has an impact on tumour levels on
 284 both $t = 40$ and $t = 60$.

285 *Tumour sensitivity to polarisation/re-polarisation rates.* In Figure 6 we show
 286 the magnitude of changes in tumour size on days $t = 40$ (panel (a)) and $t = 60$

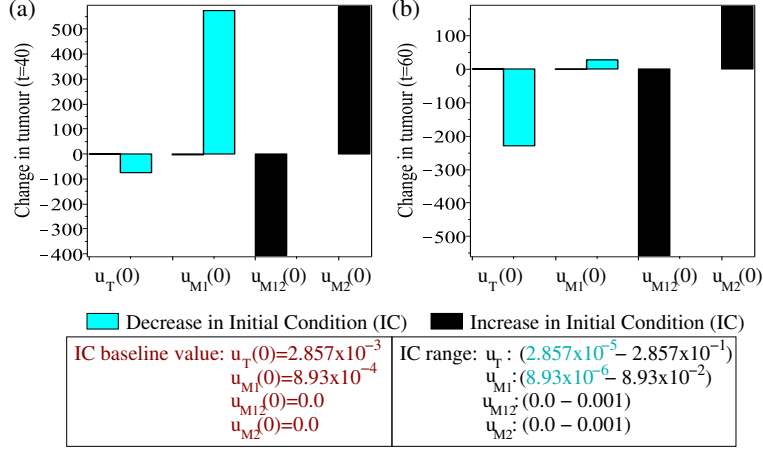


Figure 5: Changes in tumour size (see L_S in eq. (4)) on days (a) $t = 40$ and (b) $t = 60$, as we vary the initial conditions (ICs) for each of the four variables from their baseline values (in red colour) to the lower values (cyan colour) and the upper values (black colour) of the indicated IC ranges. Since the baseline values for $u_{M12}(0)$ and $u_{M2}(0)$ were zero, we only increased these values to 10^{-3} .

287 (panel (b)), as we vary separately each of the rates α_{m1} , α_{m12} , α_{m21} , α_{m2} . The
 288 rates α_{m1} , α_{m12} are increased/decreased by 90% from their baseline levels, while
 289 rates α_{m2} , α_{m21} are increased from their zero baseline levels to 0.01. Panels
 290 (c),(d),(e) show the time evolution of tumour ($t \in [0, 100]$) as we vary these
 291 rates polarisation/re-polarisation rates. As expected, when we decrease α_{m12}
 292 or we increase α_{m2} we see a decrease in tumour size. However, unexpectedly,
 293 a decrease in α_{m1} (which should reduce the M1→M2 polarisation), seems to
 294 cause a significant increase in the tumour population.

295 In Figure 7 we show the effect of varying at the same time and by the same
 296 amount the polarisation rates α_{m1} and α_{m12} (where we assume that $\alpha_{m1} =$
 297 $\alpha_{m12} =: \alpha_1$), and the re-polarisation rates α_{m2} and α_{m21} (where we assume
 298 that $\alpha_{m2} = \alpha_{m21} =: \alpha_2$). Panels (a) and (b) show the magnitude of the changes
 299 in tumour size on days $t = 40$ and $t = 60$, while panels (c) and (d) show the time-
 300 variations in $u_T(t)$ as we vary simultaneously $\alpha_{m1} = \alpha_{m12}$ and $\alpha_{m2} = \alpha_{m21}$,
 301 respectively.

- 302 • Figure 7(c): when we decrease $\alpha_{m1} = \alpha_{m12} = \alpha_1$ to $\alpha_1 = 0.00001$ we first
 303 observe a tumour increase (for $t \in (30, 50)$) followed by a large decrease
 304 (for $t \in (50, 80)$). The initial tumour increase is unexpected, since a
 305 reduction in α_1 should keep the macrophages in a M1-like phenotype.
- 306 • Figure 7(d): when we increase $\alpha_{m2} = \alpha_{m21} = \alpha_2$, we observe that
 307 the tumour can be reduced and eventually eliminated for very large re-
 308 polarisation rates (e.g., $\alpha_2 = 0.2$). However, in the short time ($t \in (30, 50)$)
 309 the tumour grows to large sizes; it can even reach its carrying capacity
 310 before being killed by the M1-like macrophages. Therefore, these results

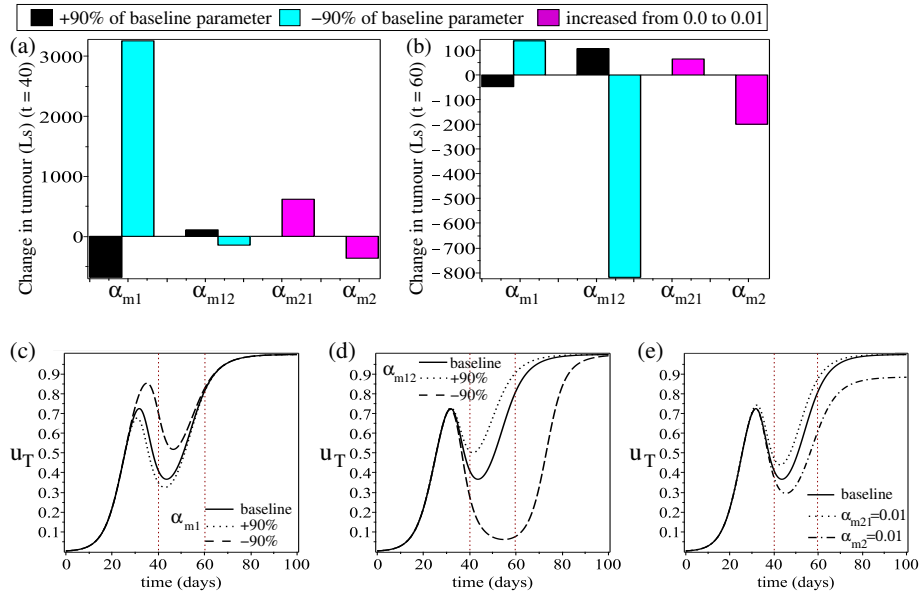


Figure 6: Changes in tumour size (see L_s in eq. (4)) on days (a) $t = 40$ and (b) $t = 60$, as we vary separately α_{m1} , α_{m12} by $\pm 90\%$ from their baseline values (black and cyan colours), while α_{m21} and α_{m2} are increased separately from 0.0 to 0.01 (magenta colour). In (c), (d) we show the time-evolution of the tumour as vary separately by $\pm 90\%$ (c) α_{m1} and (d) α_{m12} . In (e) we show the time-evolution of the tumour as we vary separately α_{m21} and α_{m2} : each rate is increased from 0.0 (baseline) to 0.01. The dotted vertical lines indicate the times $t = 40$ and $t = 60$.

311 suggests that there might be a range for the re-polarisation rates that
 312 would lead to optimal treatment. (For murine experiments mice are killed
 313 for humane reasons when the tumours grow too large, and thus a potential
 314 tumour decay for $t > 80$ would not be observed).

315 To further investigate the unexpected effect of α_{m1} on tumour growth, in Figure
 316 8 we show the tumour cell volume as we vary: (a) d_{t1} (to verify whether
 317 tumour increase for low α_{m1} is the result of low M1 phagocytosis); (b) $u_{M1}(0)$
 318 (to verify whether tumour increase for low α_{m1} is the result of low initial M1
 319 population); (c) d_{m1} (to verify whether tumour increase is the result of a con-
 320 tinuously low M1 population due to high death rate). It is clear that while an
 321 increase in d_{t1} and $u_{M1}(0)$ alone, or a decrease in d_{m1} alone, leads to a tempo-
 322 rary reduction in tumour size, when we combine them also with a decrease in
 323 α_{m1} the tumour grows back. A more significant tumour reduction is observed
 324 for very low d_{m1} values (i.e., $d_{m1} \leq 0.5$). Only in this particular case, a de-
 325 crease in α_{m1} leads to lower tumour sizes – although the tumour will eventually
 326 relapse and grow to its carrying capacity. This temporary decrease in tumour
 327 size seems to be the result of higher $\%u_{M12}$ (see Figure 8(c)(ii)-(ii')).

328 Since macrophages death rates seem to play an important role in macrophage
 329 re-polarising treatments, in Figure 9 we explore the region in the (d_{m12}, d_{m1})

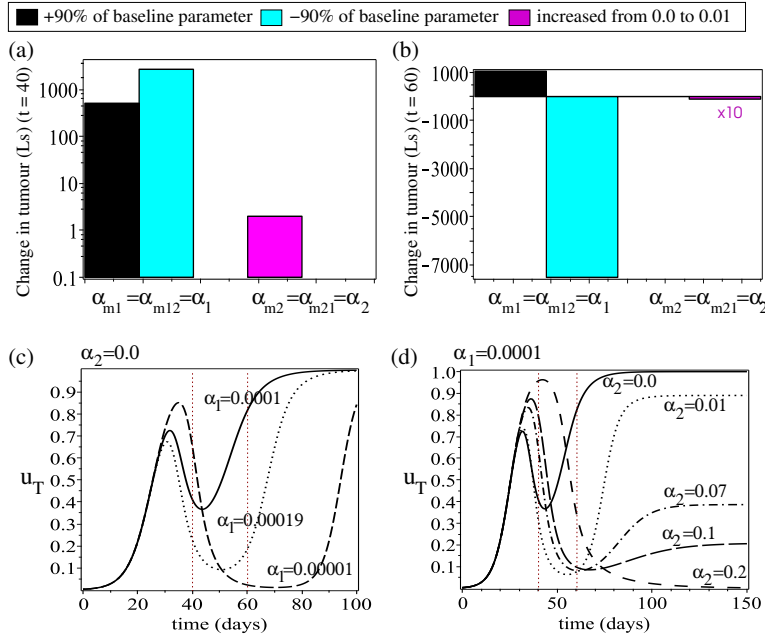


Figure 7: Panels (a),(b) show changes in tumour size (i.e., L_S value given by eq. (4)) on days $t = 40$ and $t = 60$, as we vary at the same time the two polarisation rates $\alpha_{m1} = \alpha_{m12} =: \alpha_1$ by $\pm 90\%$ (from a common baseline value of $\alpha_1 = 0.0001$) and $\alpha_{m2} = \alpha_{m21} =: \alpha_2$ (from their baseline value 0.0 to 0.01). Since the increase in α_2 has a very little effect on tumour size on day $t = 60$, to improve the visualisation we multiplied the value L_S from eq. (4) by a factor of 10. Panel (c) shows the time-evolution of u_T when we assume $\alpha_{M2} = \alpha_{M21} = 0.0$ and we vary $\alpha_1 := \alpha_{M1} = \alpha_{M12}$. Panel (d) shows the time-evolution of u_T when we assume $\alpha_{M1} = \alpha_{M12} = 0.0001$ and we vary $\alpha_2 := \alpha_{M2} = \alpha_{M21}$. The dotted vertical lines indicate the times $t = 40$ and $t = 60$.

330 space for which a decrease in α_{m1} (from 10^3 to 10^4) leads to a decrease or an
 331 increase in tumour size. The thick red curve in the top-left panel corresponds to
 332 a stationary tumour (i.e. the dot and dash-dot curves overlap, and the tumour
 333 is neither increasing nor decreasing). For three cases corresponding to three cor-
 334 ners of this main panel, we show both the time-evolution of the tumour, and the
 335 percentage of macrophages corresponding to some of these tumours. We observe
 336 that tumour reduction/control for $d_{m12} = 0.14$, $d_{m1} = 0.45$ is associated with a
 337 large percentage of macrophages with mixed M1/M2 phenotypes. In contrast,
 338 tumour reduction/control for $d_{m12} = 0.35$, $d_{m1} = 0.45$ is associated with a very
 339 low percentage of macrophages with mixed M1/M2 phenotypes. Hence, the
 340 death rates of macrophages with M1-like phenotype or mixed M1/M2-like phe-
 341 notype seem to play an important role on tumour growth/control/decay, and
 342 on the percentage of mixed macrophages during tumour growth/control/decay.
 343 We will discuss these results in more detail in Section 4.

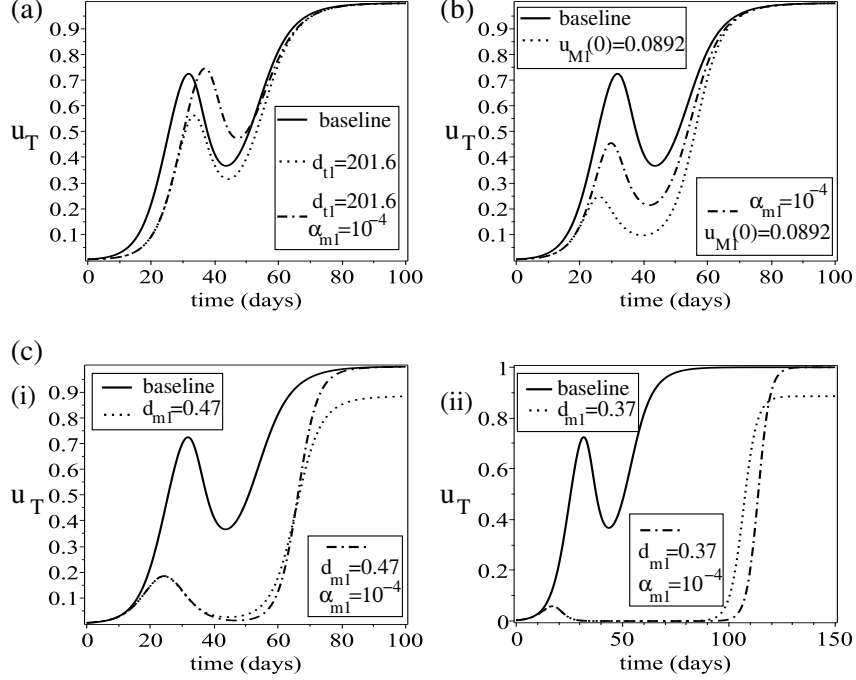


Figure 8: Time-evolution of tumour cell volume as we vary different parameters related to M1 cells. The “baseline” case (continuous curve) corresponds to the parameter values listed in Table 2.1, where $\alpha_{m1} = 10^{-3}$. (a) Vary d_{t1} alone (dotted curve) or in combination with α_{m1} (dash-dot curve). To see some difference in tumour dynamics, we had to increase d_{t1} by a factor of 30: from $d_{t1} = 1.344$ to $d_{t1} = 201.6$ (b) Vary the initial condition $u_{M1}(0)$ alone (dashed-dot curve) or in combination with α_{m1} (dash-dot curve). Here we increased the initial condition by a factor of 100: from $u_{M1}(0) = 0.000892$ to $u_{M1}(0) = 0.0892$. (c) Vary d_{m1} alone (dotted curve) or in combination with α_{m1} (dash-dot curve). Here we show the effects of medium vs. low values of d_{m1} : (i) $d_{m1} = 0.6$, (ii) $d_{m1} = 0.5$. For this panel (c) we also show the percentage of various types of macrophages: (i') for the case $d_{m1} = 0.6$, (ii') for the case $d_{m1} = 0.5$.

344 3.2.2. Global sensitivity analysis

345 To determine the impact that possible interactions between multiple uncer-
 346 tain parameters have on overall tumour dynamics, next we perform a global
 347 sensitivity and uncertainty analysis using the classical LHS/PRCC (Latin Hy-
 348 percube Sampling/Partial Rank Correlation Coefficient) approach [40, 41].

349 In Figure 10 we show the results of a global sensitivity and uncertainty anal-
 350 ysis for: (a) tumour population (u_T), (b) M1 macrophage population (u_{M1}),
 351 (c) macrophage population with mixed M1/M2 phenotypes (u_{M12}), and (d) M2
 352 macrophage population (u_{M2}), as we sample independently (100 times) the 14
 353 parameter values within the ranges listed in Table 2.1. Sub-panels (i) show the
 354 average population outputs (“mean” and “standard deviations” (\pm sd) in darker
 355 colours, and maximum/minimum values in lighter colours), while sub-panels (ii)

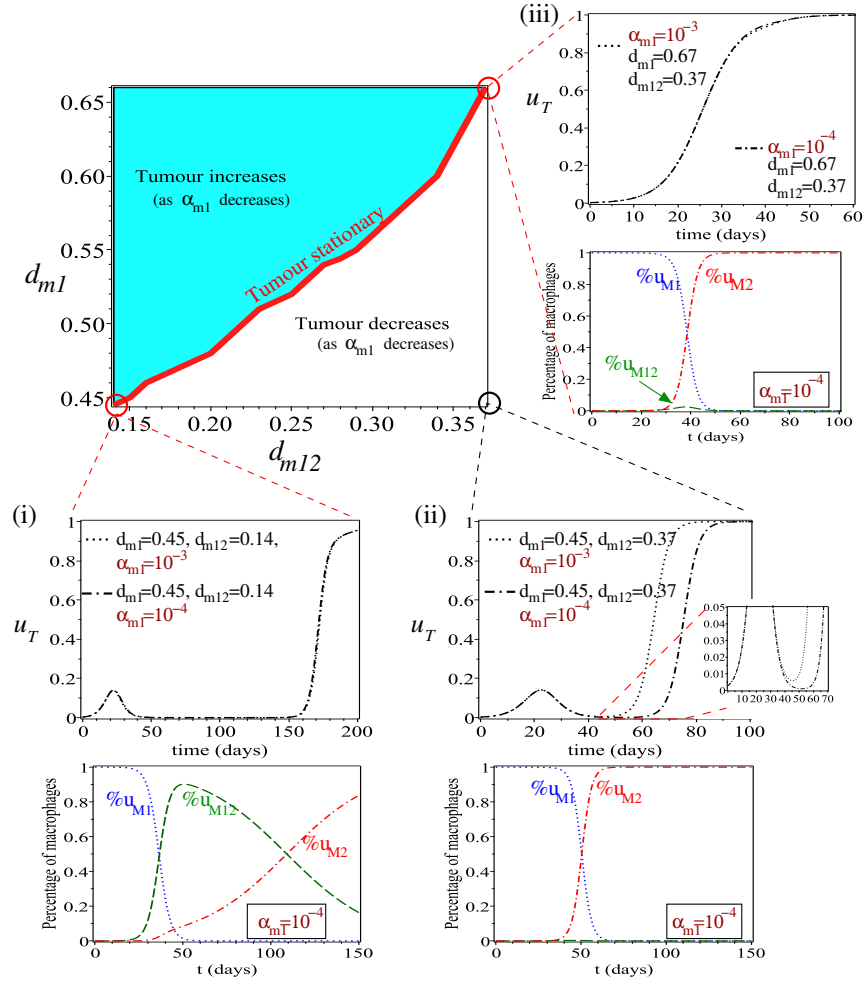


Figure 9: Bifurcation diagram in the (d_{m12}, d_{m1}) parameter space showing the regions where a decrease in α_{m1} from 10^{-3} (dot curves) to 10^{-4} (dash-dot curves) leads to a decrease in tumour size (white region) or an increase in tumour size (cyan region). To make it clear what we mean by stationary tumour (i.e. the dot and dash-dot curves overlap), we also show the time-evolution of the tumour and macrophage percentage at three corner points in this parameter space: (i) $d_{m12} = 0.14$, $d_{m1} = 0.45$; (ii) $d_{m12} = 0.37$, $d_{m1} = 0.45$; and (iii) $d_{m12} = 0.37$, $d_{m1} = 0.67$. To clarify that the delay in tumour relapse observed for case (ii) is the result of reduced tumour levels, in this sub-figure we also show a zoom-in of tumour growth curves for $u_T < 0.05$.

356 show the PRCC values. For the PRCC analysis, we note that the parameters
 357 with large PRCC absolute values are the most important. In particular, values
 358 closer to ± 1 indicate parameters that influence strongly the outcome variable,
 359 while the sign indicates the qualitative relation between input parameters and

360 output variables (with “+” sign indicating that the parameter is directly pro-
 361 portional to the outcome, and the “-” sign indicating that the parameter is
 362 inversely proportional to the outcome). In Figure 10 we see that:

- 363 • The parameters with the largest impact on u_T are α_{m21} , α_{m2} , d_{t1} , p_{m2}
 364 and d_{m12} . Interestingly, these parameters correspond to the four tumour-
 365 associated macrophage targeted therapeutic strategies discussed in [42]:
 366 antibody-mediated elimination of tumour cells (d_{t1}), blockage of monocyte
 367 recruitment to tumours (p_{m2}), re-polarisation to an M1-like phenotype
 368 (α_{m21} , α_{m2}), and suppression of macrophage survival (d_{m12}).
- 369 • The parameters with the largest impact on u_{M1} are α_{m2} , d_{m12} , and p_{m2} .
- 370 • The parameter with the largest impact on u_{M12} is α_{m21} , followed by α_{m2} ,
 371 d_{m12} and p_{m2} .
- 372 • The parameter with the largest impact on u_{M2} are α_{m2} , followed by p_{m2} .
 373 Among the polarisation rates, the largest impact is provided by α_{m12} .

374 The above results identified the proliferation/recruitment rate of M2 macrophages
 375 (p_{m2}) as a parameter important not only for tumour dynamics, but also for
 376 the dynamics of all macrophage phenotypes, including u_{M1} and u_{M12} . There-
 377 fore, reducing p_{m2} will impact tumour growth both directly (through the direct
 378 pro-tumour effect of M2 macrophages [43, 26]) and indirectly (through the M1
 379 macrophages and macrophages with mixed M1/M2 phenotypes).

380 4. Discussion

381 In this study we developed and investigated numerically a new mathemat-
 382 ical model for the temporal dynamics between non-small cell lung cancer and
 383 macrophages in the lung, with the ultimate goal of shedding some light on the
 384 importance of macrophages with mixed phenotypes.

385 After showing the baseline dynamics of this new model (Figure 4), we started
 386 performing a local sensitivity analysis, to gain some understanding of the effects
 387 of changes in the initial conditions (Figure 5), as well as changes in those param-
 388 eters describing macrophage polarisation/re-polarisation rates (Figures 6 - 9).
 389 In regard to the initial conditions, our local sensitivity analysis showed that the
 390 most important role is played by $u_{M12}(0)$. For the baseline parameter values
 391 investigated in this study (see Table 2.1) we observed that a decrease in the
 392 polarisation rate α_{m12} (i.e., $u_{M1} \rightarrow u_{M12}$ polarisation) led to larger tumours,
 393 even when we increased the initial level of M1 macrophages ($u_{M1}(0)$) or the M1
 394 macrophages phagocytosis rate (d_{t1}). We discovered that this was the result of
 395 short half-life of M1 cells (i.e., large d_{m1} ; see Figures 8 - 9).

396 Returning to Figure 1(a), one of the main questions of this paper was to
 397 shed some light on the role of macrophages with mixed phenotypes on tumour
 398 elimination/growth. Through numerical simulations in Figures 8-9, we showed
 399 that the percentage of u_{M12} macrophages depends on the elimination rates d_1

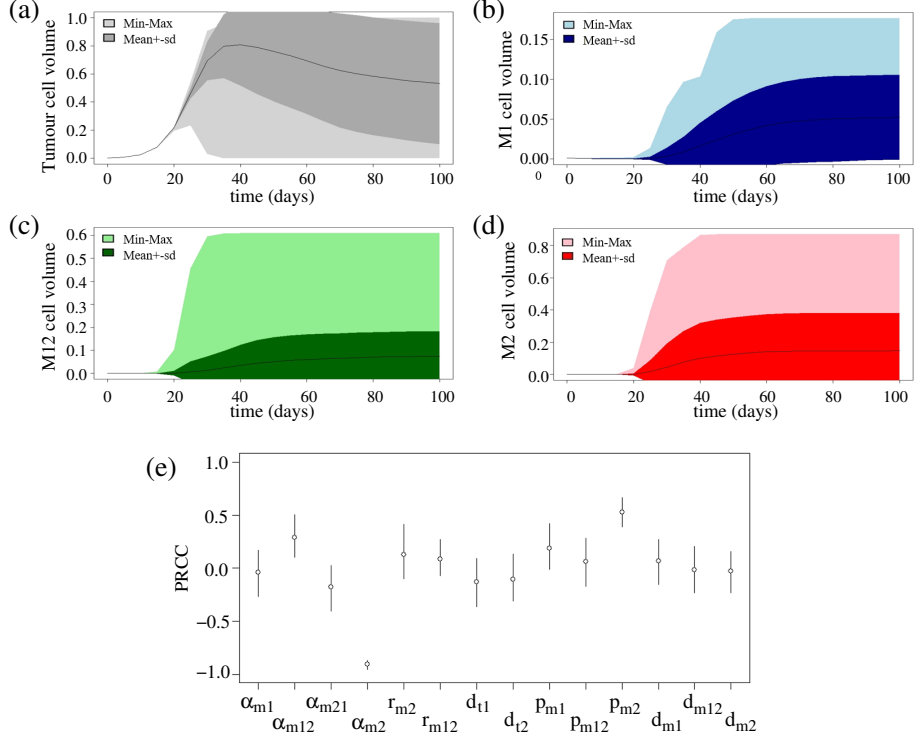


Figure 10: Global sensitivity and uncertainty analysis for variables (a) u_T , (b) u_{M1} , (c) u_{M12} , (d) u_{M2} as we vary 14 parameters within the ranges specified in Table 2.1. Sub-panels (i) show the mean+standard deviation, together with max/min values of these variables as we vary t . Sub-panels (ii) show the PRCC values corresponding to each of the parameters varied in Table 2.1.

400 and d_{12} (and it probably on other parameters as well). In particular, tumour
 401 decay/control can occur for both low and high u_{M12} percentages. Therefore,
 402 our theoretical study suggests that unless we know exactly the elimination rates
 403 of macrophages with different phenotypes (M1 or mixed M1/M2) we cannot use
 404 the macrophages with mixed phenotypes as predictors of tumour elimination
 405 (and patient survival).

406 The results presented in this study depend heavily on the parameters used
 407 for the simulations. Some of these parameter values were obtained from in-vitro
 408 and ex-vivo experiments [30, 33], and therefore they could be different from the
 409 in-vivo murine parameters and even more from the in-vivo human parameters.
 410 Unfortunately, we do not have in-vivo data to parametrise these mathemati-
 411 cal models, and our best approach was a sensitivity and uncertainty analysis
 412 to understand the extent of variations in model outcomes. Global sensitivity

413 analysis (Figure 10) revealed the parameters with the largest impact for tumour
414 dynamics (α_{m21} , α_{m2} , d_{t1} , p_{m2} and d_{m12}), and interestingly these parameters
415 were also the parameters involved in four of the macrophage-targeted treat-
416 ment approaches for cancer as identified in [42]: re-polarisation of macrophages
417 towards an M1-like phenotype (α_{m21} , α_{m2}), suppression of tumour-associated
418 macrophages survival (d_{m12}), blockade of macrophage recruitment (p_{m2}), and
419 antibody-mediated elimination of tumour cells by macrophages (d_{t1}).

420 Overall, the results of this study emphasise the need for a better experi-
421 mental understanding of the kinetics (doubling time, half lives) of macrophages
422 with different phenotypes that can be found inside solid tumours (especially
423 the macrophages with mixed phenotypes). Most of the experimental studies
424 in the literature focus on the kinetics of T cells [44, 45], but given the im-
425 portance of tumour-associated macrophages on tumour evolution, more exper-
426 imental studies are necessary to better understand the macrophage kinetics.
427 Unfortunately, the lack of robust macrophage markers can lead to inaccurate
428 macrophage counts [16], which further impacts our hope of reliable data on
429 macrophage kinetics. Until more data will become available, we have to continue
430 using modelling and computational approaches to propose hypotheses regarding
431 the macrophage dynamics and their interactions with various components of the
432 tumour microenvironment.

433 **Appendix A. Spatially-homogeneous steady states**

434 We have seen in Figures 7(d) and 8(c),(d) that changes in some parameters
 435 can lead to lower tumour sizes in the long term (for $\alpha_{m21}, \alpha_{m2} > 0$), in contrast
 436 to the case α . To understand better this long-term dynamics of model (1), in the
 437 following we summarise the steady states exhibited by this model by focusing
 438 on two case: (i) the baseline case characterised by $\alpha_{m2} = \alpha_{m21} = 0$, and (ii) the
 439 treatment case characterised by $\alpha_{m2}, \alpha_{m21} > 0$.

440 **Proposition 1.** *For the baseline case (i) with $\alpha_{m2}, \alpha_{m21} = 0$, model (1) can*
 441 *exhibit the following steady states:*

- 442 • *Tumour-Free Immune-Free (TFIF) state: $(u_T^*, u_{M1}^*, u_{M12}^*, u_{M2}^*) = (0, 0, 0, 0)$,*
 443 *which exists for all parameter values;*
- 444 • *Tumour-Free M2-Present (TFM2P) steady state: $(u_T^*, u_{M1}^*, u_{M12}^*, u_{M2}^*) =$*
 445 *$(0, 0, 0, \frac{K_m(p_{m2} - d_{m2})}{p_{m2}})$, which exists for $p_{m2} > d_{m2}$;*
- 446 • *Tumour-Free M12-Present (TFM12P) steady state: $(u_T^*, u_{M1}^*, u_{M12}^*, u_{M2}^*)$*
 447 *$= (0, 0, \frac{K_m(p_{m12} - d_{m12})}{p_{m12}}, 0)$, which exists for $p_{m12} > d_{m12}$;*
- 448 • *Tumour-Free M1-Present (TFM1P) steady state: $(u_T^*, u_{M1}^*, u_{M12}^*, u_{M2}^*) =$*
 449 *$(0, \frac{K_m(p_{m1} - d_{m1})}{p_{m1}}, 0, 0)$, which exists only for $p_{m1} > d_{m1}$, an inequality not*
 450 *satisfied by the baseline parameter values in Table 2.1;*
- 451 • *Tumour-Present Immune-Free (TPIF) steady state: $(u_T^*, u_{M1}^*, u_{M12}^*, u_{M2}^*)$*
 452 *$= (K_t, 0, 0, 0)$, which exists for all parameter values;*
- 453 • *Tumour-Present M2-Present (TPM2P) steady state: $(u_T^*, u_{M1}^*, u_{M12}^*, u_{M2}^*)$*
 454 *$= (K_t, 0, 0, \frac{p_{m2} - d_{m2}}{p_{m2}} K_m)$ which exists for $p_{m2} > d_{m2}$;*
- 455 • *Tumour-Present M12-M2-Present (TPM12M2P) steady state: $(u_T^*, u_{M1}^*, u_{M12}^*, u_{M2}^*)$*
 456 *$= (u_T^*, 0, u_{M12}^*, u_{M2}^*)$ with the non-zero states connected via the following*
 457 *equations:*

$$u_{M12}^* = \frac{K_m \frac{[p_{m12}(u_T^* + K_t^*) - d_{m12}(u_T^* + K_t^*) + \alpha_{m12}u_T^*]}{p_{m12}(u_T^* + K_t^*)}}{\frac{\alpha_{m12}u_T^*}{(u_T^* + K_t^*)p_{m2} \left[\frac{d_{m12}}{p_{m12}} - \frac{\alpha_{m12}}{p_{m12}} \frac{u_T^*}{u_T^* + K_t^*} \right] - d_{m2}(u_T^* + K_t^*)} + 1}, \quad (\text{A.1})$$

$$u_{M2}^* = K_m \left(1 - \frac{d_{m12}}{p_{m12}} + \frac{\alpha_{m12}}{p_{m12}} \frac{u_T^*}{u_T^* + K_t^*} \right) - u_{M12}^*, \quad (\text{A.2})$$

$$0 = p_t \left(1 - \frac{u_T^*}{K_t} \right) (1 + r_{m2}u_{M2}^* + r_{m12}u_{M12}^*) - d_{t2}u_{M12}^*. \quad (\text{A.3})$$

- 458 • *Tumour-Present Immune-Present (TPIP) steady state: $(u_T^*, u_{M1}^*, u_{M12}^*, u_{M2}^*)$.*

459 **Proposition 2.** *For the case (ii) when a macrophage re-polarisation treatment*
 460 *is considered (i.e., $\alpha_{m2}, \alpha_{m21} > 0$), model (1) can exhibit the following tumour-*
 461 *free and tumour-present steady states:*

- 462 • *Tumour-Free Immune-Free (TFIF) state:* $(u_T^*, u_{M1}^*, u_{M12}^*, u_{M2}^*) = (0, 0, 0, 0)$,
 463 *which exists for all parameter values;*
- 464 • *Tumour-Free M1-cells Present (TFM1P) state:* $(u_T^*, u_{M1}^*, u_{M12}^*, u_{M2}^*) =$
 465 $(0, K_m \frac{p_{m1} - d_{m1}}{p_{m1}}, 0, 0)$, *which exists only if* $p_{m1} > d_{m1}$.
- 466 • *Tumour-Free M2-cells Free (TFM2F) state:* $(u_T^*, u_{M1}^*, u_{M12}^*, u_{M2}^*) = (0, u_{M1}^*, u_{M12}^*, 0)$,
 467 *with*

$$u_{M1}^* = \frac{\alpha_{m21} K_m (\alpha_{m21} + d_{m12} - p_{m12})}{(p_{m1} - p_{m12}) \alpha_{m21} - d_{m1} p_{m12} + d_{m12} p_{m1}},$$

$$u_{M12}^* = \frac{K_m (d_{m12} + \alpha_{m21} - p_{m12}) (-d_{m1} p_{m12} + p_{m1} (d_{m12} + \alpha_{m21}))}{p_{m12} (p_{m12} (d_{m1} + \alpha_{m21}) - p_{m1} (d_{m12} + \alpha_{m21}))}.$$

- 468 • *Tumour-Free, Immune response Present (TFIP) state:* $(u_T^*, u_{M1}^*, u_{M12}^*, u_{M2}^*)$
 469 $= (0, u_{M1}^*, u_{M12}^*, u_{M2}^*)$, *with*

$$u_{M1}^* = \frac{\alpha_{m2} \alpha_{m21} K_m p_{m2} (d_{m2} + \alpha_{m2} - p_{m2})}{((-d_{m1} - \alpha_{m21}) \alpha_{m2} - d_{m1} (\alpha_{m21} + d_{m12})) p_{m2}^2 - p_{m1} p_{m12} (d_{m2} + \alpha_{m2})^2 + (d_{m2} + \alpha_{m2}) (p_{m1} \alpha_{m2} + (\alpha_{m21} + d_{m12}) p_{m1} + d_{m1} p_{m12}) p_{m2}}$$

470

$$u_{M12}^* = \frac{\alpha_{m2} (-d_{m1} p_{m2} + p_{m1} (\alpha_{m2} + d_{m2})) (\alpha_{m2} + d_{m2} - p_{m2}) K_m}{((-d_{m1} - \alpha_{m21}) \alpha_{m2} - d_{m1} (\alpha_{m21} + d_{m12})) p_{m2}^2 - p_{m1} p_{m12} (\alpha_{m2} + d_{m2})^2 + (\alpha_{m2} + d_{m2}) (p_{m1} \alpha_{m2} + (\alpha_{m21} + d_{m12}) p_{m1} + d_{m1} p_{m12}) (\alpha_{m2} + d_{m2}) p_{m2}}$$

471 *and*

$$u_{M2}^* = \frac{[p_{m1} (\alpha_{m2} + d_{m2}) - d_{m1} p_{m2}] (\alpha_{m2} + d_{m2} - p_{m2}) \cdot ((-\alpha_{m21} - d_{m12}) p_{m2} + p_{m12} (\alpha_{m2} + d_{m2})) K_m}{p_{m2} (((-d_{m1} - \alpha_{m21}) \alpha_{m2} - d_{m1} (\alpha_{m21} + d_{m12})) p_{m2}^2 - p_{m1} p_{m12} (\alpha_{m2} + d_{m2})^2) + p_{m2} ((\alpha_{m2} + \alpha_{m21} + d_{m12}) p_{m1} + d_{m1} p_{m12}) (\alpha_{m2} + d_{m2}) p_{m2}}$$

- 472 • *Tumour-Present Immune-Free (TPIF) state:* $(u_T^*, u_{M1}^*, u_{M12}^*, u_{M2}^*) = (K_t, 0, 0, 0)$,
 473 *which exists for all parameter values;*

- 474 • *Tumour-Present M1, M12 and M2 Immune response Present (TPIP) state:*
 475 $(u_T^*, u_{M1}^*, u_{M12}^*, u_{M2}^*) = (u_T^*, u_{M1}^*, u_{M12}^*, u_{M2}^*)$.

476 **Remark 3.** *Both cases investigated above, namely (i) no re-polarising treat-*
 477 *ment* $(\alpha_{m2} = \alpha_{m21} = 0)$ *and (ii) re-polarising treatment* $(\alpha_{m2}, \alpha_{m21} > 0)$ *had*
 478 *a tumour-only steady state (TPIF) and coexistence steady states (TPIP). How-*
 479 *ever, case (i) can exhibit two other steady states characterised by the presence*
 480 *of tumour cells and the absence of M1-like cells* $(u_{M1}^* = 0)$: *the TPM2P and*
 481 *TPM12M2P states. This suggests that in the absence of any external treatment*
 482 *to re-polarise the macrophages towards an M1-like phenotype, the tumours are*
 483 *always formed of M2-like macrophages or macrophages with a mixed M1/M2*
 484 *phenotype.*

485 *Stability of steady states.* The linear stability of the above steady states is controlled by the eigenvalues of the Jacobian matrix associated with the system
 486 (1):
 487

$$J(u_T^*, u_{M1}^*, u_{M12}^*, u_{M2}^*) = \begin{pmatrix} a_{11} & a_{12} & a_{13} & a_{14} \\ a_{21} & a_{22} & a_{23} & a_{24} \\ a_{31} & a_{32} & a_{33} & a_{34} \\ a_{41} & a_{42} & a_{43} & a_{44} \end{pmatrix}, \quad \text{with}$$

$$\begin{aligned} a_{11} &= p_t \left(1 - \frac{2u_T^*}{K_t}\right) (r_{m12}u_{M12}^* + r_{m2}u_{M2}^* + 1) - d_{t1}u_{M1}^* - d_{t2}u_{M12}^*, \\ a_{12} &= -d_{t1}u_T^*, \\ a_{13} &= p_t u_T^* \left(1 - \frac{u_T^*}{K_t}\right) r_{m12} - d_{t2}u_T^*, \\ a_{14} &= p_t u_T^* \left(1 - \frac{u_T^*}{K_t}\right) r_{m2}, \\ a_{21} &= \frac{\alpha_{m1}u_{M1}^*}{u_T^* K_t^*} \left(\frac{u_T^*}{u_T^* + K_t^*} - 1\right), \\ a_{22} &= p_{m1} \left(1 - \frac{u_{M1}^* + u_{M12}^* + u_{M2}^*}{K_m}\right) - \frac{p_{m1}}{u_{M1}^*} - d_{m1} - \frac{\alpha_{m1}u_T^*}{u_T^* + K_t^*}, \\ a_{23} &= -\frac{p_{m1}u_{M1}^*}{K_m} + \alpha_{m21}, \\ a_{24} &= -\frac{p_{m1}u_{M1}^*}{K_m}, \\ a_{31} &= \frac{\alpha_{m1}u_{M1}^*}{u_T^* + K_t^*} \left(1 - \frac{u_{M1}^*}{u_T^* + K_t^*}\right) + \frac{\alpha_{m12}u_{M12}^*}{u_T^* + K_t^*} \left(\frac{u_{M12}^*}{u_T^* + K_t^*} - 1\right), \\ a_{32} &= \frac{\alpha_{m1}u_T^*}{u_T^* + K_t^*} - \frac{p_{m12}u_{M12}^*}{K_m}, \\ a_{33} &= p_{m12} \left(1 - \frac{u_{M1}^* + 2u_{M12}^* + u_{M2}^*}{K_m}\right) - d_{m12} - \alpha_{m21} - \frac{\alpha_{m12}u_T^*}{u_T^* + K_t^*}, \\ a_{34} &= \alpha_{m2} - \frac{p_{m12}u_{M12}^*}{K_m}, \\ a_{41} &= \frac{\alpha_{m12}u_{M12}^*}{u_T^* + K_t^*} \left(1 - \frac{u_T^*}{u_T^* + K_t^*}\right), \\ a_{42} &= -\frac{p_{m2}u_{M2}^*}{K_m}, \\ a_{43} &= \frac{\alpha_{m12}u_T^*}{u_T^* + K_t^*} - \frac{p_{m2}u_{M2}^*}{K_m}, \\ a_{44} &= p_{m2} \left(1 - \frac{u_{M1}^* + u_{M12}^* + u_{M2}^*}{K_m}\right) - \frac{p_{m2}u_{M2}^*}{K_m} - d_{m2} - \alpha_{m2}. \end{aligned}$$

488 **Proposition 3.** *The steady states exhibited by model (1) for the baseline case*
 489 $\alpha_{m2} = \alpha_{m21} = 0$ *have the following linear stability:*

- 490 • The TFIF state is always unstable.
- 491 • The TFM2P state is always unstable when it exists (i.e., for $p_{m2} > d_{m2}$).
- 492 • The TFM12P state is stable provided that $\frac{d_{m12}}{p_{m12}} < \min\{\frac{d_{m2}}{p_{m2}}, \frac{d_{m1}}{p_{m1}}\}$, and
493 $p_{t1}r_{m12} < d_{t2}$.
- 494 • The TFM1P state is stable provided that $\frac{d_{m1}}{p_{m1}} < \min\{\frac{d_{m2}}{p_{m2}}, \frac{d_{m12}}{p_{m12}}\}$ and
495 $p_{t1}p_{m1} < d_{t1}K_m(p_{m1} - d_{m1})$.
- 496 • The TPIF state is stable provided that $p_{m2} < d_{m2}$ and $p_{m1} < d_{m1}$ and
497 $p_{m12} < d_{m12}$.
- 498 • The TPM2P state is stable provided that $\frac{d_{m2}}{p_{m2}} < \min\{\frac{d_{m1}}{p_{m1}}, \frac{d_{m12}}{p_{m12}}\}$.

499 The stability of TPM12M2P and TPIP states (for the case $\alpha_{m2} = \alpha_{m21} = 0$)
500 is more difficult to investigate for general parameters. Also the stability of the
501 steady states corresponding to the case $\alpha_{m2}, \alpha_{m21} > 0$ is difficult to investigate
502 for the general parameters (the exceptions being the TFIF and TFM1P states,
503 whose stability is given by the same conditions as in Proposition 3). For these
504 reasons, the following Remark summarises the stability of all steady states for
505 the baseline parameter values in Table 2.1.

506 **Remark 4.** For the baseline parameter values given in Table 2.1 (with $\alpha_{m2} =$
507 $\alpha_{m21} = 0$), the steady states TFM1P, TPM12M2P and TPIP do not exist.
508 The stability of the existent steady states is as follows: the TFIF state is unstable
509 (saddle), the TFM2P state is unstable (saddle), the TFM12P state is unstable
510 (saddle), the TPIF state is unstable (saddle), and the TPM2P state is stable
511 (node). These results explain the dynamics observed in Figure 4, where the
512 solutions approach the only stable steady state: the TPM2P state.

513 For the case $\alpha_{m2} = \alpha_{m21} = 0.1$ (and the rest of parameters as in Table 2.1),
514 the steady state TFM1P does not exist.

515 The stability of the existent steady states is as follows: the TFIF state is unsta-
516 ble (saddle), the TFM2F state is unstable (saddle), the TFIP state is unstable
517 (saddle), the TPIF state is unstable (saddle), and TPIP is stable (node). This
518 explains the dynamics observed in Figure 7(d), where the solutions approach the
519 only stable steady state: the TPIP state.

- 520 [1] D. Carbone, D. Gandara, S. Antonia, C. Zielinski, L. Paz-Ares, Non-small
521 cell lung cancer: role of the immune system and potential for immunother-
522 apy, J. Thorac. Oncol. 10 (7) (2015) 974–984.
- 523 [2] C. Gridelli, A. Rossi, D. Carbone, J. Guarize, N. Karachaliou, T. Mok,
524 F. Petrella, L. Spaggiari, R. Rosell, Non-small-cell lung cancer, Nature
525 Reviews 1 (2015) 15009.
- 526 [3] B. Stankovic, H. Bjøhovde, R. Skarshaug, H. Aamodt, A. Frafjord,
527 E. Müller, C. Hammarström, K. Beraki, E. Baekkevold, P. Woldbaek,

- 528 A. Helland, O. Brustugun, I. Øynebråten, A. Corthay, Immune cell com-
529 position in human non-small cell lung cancer, *Frontiers in Immunology* 3
530 (2019) 3101.
- 531 [4] J. Kargl, S. Busch, G. Yang, K.-H. Kim, M. Hanke, H. Metz, J. Hubbard,
532 S. Lee, D. Madtes, M.W.McIntosh, A. M. Houghton, Neutrophils dominate
533 the immune cell composition in non-small cell lung cancer, *Nat. Commun.*
534 8 (2017) 14381.
- 535 [5] F. Dai, L. Liu, G. Che, N. Yu, Q. Pu, S. Zhang, J. Ma, L. Ma, Z. You,
536 The number and microlocalisation of tumour-associated immune cells are
537 associated with patient's survival time in non-small cell lung cancer, *BMC*
538 *Cancer* 10 (2010) 220.
- 539 [6] M. Tamminga, T. Hiltermann, E. Schuurung, W. Timens, R. Fehrmann,
540 Immune microenvironment composition in non-small cell lung cancer and
541 its association with survival, *Clinical & Translational Immunology* 9 (2020)
542 e1142.
- 543 [7] A. Mantovani, S. Sozzani, M. Locati, P. Allavena, A. Sica, Macrophage
544 polarization: tumor-associated macrophages as a paradigm for polarized
545 m2 mononuclear phagocytes, *Trends in Immunology* 23 (11) (2002) 549–
546 555.
- 547 [8] J. Ma, L. Liu, G. Che, N. Yu, F. Dai, Z. You, The m1 form of tumor-
548 associated macrophages in non-small cell lung cancer is positively associ-
549 ated with survival time, *BMC cancer* 10 (1) (2010) 112.
- 550 [9] C. Ohri, A. Shikotra, R. Green, D. Waller, P. Bradding, Macrophages
551 within nscLc tumour islets are predominantly of a cytotoxic m1 phenotype
552 associated with extended survival, *European Respiratory Journal* 33 (1)
553 (2009) 118–126.
- 554 [10] L. Cao, X. Che, X. Qiu, Z. Li, B. Yang, S. Wang, K. Hou, Y. Fan, X. Qu,
555 Y. Liu, M2 macrophage infiltration into tumor islets leads to poor prognosis
556 in non-small-cell lung cancer, *Cancer Management and Research* 11 (2019)
557 6125.
- 558 [11] J. Jackute, M. Zemaitis, D. Pranys, B. Sitkauskiene, S. Miliauskas,
559 S. Vaitkiene, R. Sakalauskas, Distribution of m1 and m2 macrophages in tu-
560 mor islets and stroma in relation to prognosis of non-small cell lung cancer,
561 *BMC Immunology* 19 (1) (2018) 3.
- 562 [12] M. Rakaee, L.-T. R. Busund, S. Jamaly, E.-E. Paulsen, E. Richardsen,
563 S. Andersen, S. Al-Saad, R. Bremnes, T. Donnem, T. Kilvaer, Prognostic
564 value of macrophage phenotypes in resectable non-small cell lung cancer
565 assessed by multiplex immunohistochemistry, *Neoplasia* 21 (3) (2019) 282–
566 293.

- 567 [13] Z. Xu, Y. Gu, C.-Z. Wang, Y. Jin, X. Wen, J.-C. Ma, L. Tang, Z. Mao,
568 J. Qian, J. Lin, The M2 macrophage marker CD206: a novel prognos-
569 tic indicator for acute myeloid leukemia, *Oncoimmunology* 9 (1) (2020)
570 e1683347.
- 571 [14] S. Singhal, J. Stadanlick, M. Annunziata, A. Rao, P. Bhojnarwala,
572 S. O'Brien, E. Moon, E. Cantu, G. Danet-Desnoyers, H.-J. Ra, L. Litzky,
573 T. Akimova, U. Beier, W. Hancock, S. Albelda, E. Eruslanov, Human
574 tumor-associated monocytes/macrophages and their regulation of T cell
575 responses in early-stage lung cancer, *Sci. Transl. Med.* 11 (2019) 479.
- 576 [15] J. Quatromoni, E. Eruslanov, Tumour-associated macrophages: function,
577 phenotype and link to prognosis in human lung cancer, *Am. J. Transl. Res.*
578 4 (4) (2012) 376–389.
- 579 [16] S. Jayasingam, M. Citartan, T. Thang, A. Zin, E. Ch'ng, Evaluating the
580 polarisation of tumour-associated macrophages into M1 and M2, *Frontiers*
581 *in Oncology* 9 (2020) 1512.
- 582 [17] N. Almuallem, D. Trucu, R. Eftimie, Oncolytic viral therapies and the
583 delicate balance between virus-macrophage-tumour interactions: A math-
584 ematical approach, *Math. Biosci. Eng.* 18 (1) (2020) 764–799.
- 585 [18] N. Y. den Breems, R. Eftimie, The re-polarisation of m2 and m1
586 macrophages and its role on cancer outcomes, *Journal of Theoretical Biol-*
587 *ogy* 390 (2016) 23–39.
- 588 [19] R. Eftimie, H. Hamam, Modelling and investigation of the CD4⁺ T cells -
589 macrophages paradox in melanoma immunotherapies, *J. Theor. Biol.* 420
590 (2017) 82–104.
- 591 [20] R. Eftimie, Investigation into the role of macrophages heterogeneity on
592 solid tumour aggregations, *Mathematical Biosciences* 322 (2020) 108325.
- 593 [21] X. Li, M. Jolly, J. George, K. Pienta, H. Levine, Computational modeling
594 of the crosstalk between macrophage polarization and tumour cell plasticity
595 in the tumour microenvironment, *Front. Oncol.* 9 (2019) 10.
- 596 [22] F. Leonard, L. T. Curtis, M. J. Ware, T. Nosrat, X. Liu, K. Yokoi,
597 H. B. Frieboes, B. Godin, Macrophage polarization contributes to the anti-
598 tumoral efficacy of mesoporous nanovectors loaded with albumin-bound
599 paclitaxel, *Frontiers in immunology* 8 (2017) 693.
- 600 [23] F. Leonard, L. Curtis, A. Hamed, C. Zhang, E. Chau, D. Sieving, B. Godin,
601 H. Frieboes, Nonlinear response to cancer nanotherapy due to macrophage
602 interactions revealed by mathematical modeling and evaluated in a murine
603 model via CRISPR-modulated macrophage polarisation, *Cancer Immunol.*
604 *Immunother.* 69 (5) (2020) 731–744.

- 605 [24] Y. Louzoun, C. Xue, G. Lesinski, A. Friedman, A mathematical model for
606 pancreatic cancer growth and treatments, *J. Theor. Biol.* 351 (2014) 74–82.
- 607 [25] S. Benzekry, C. Lamont, A. Beheshti, A. Tracz, J. Ebos, L. Hlatky, P. Hahn-
608 nfeldt, Classical mathematical models for description and prediction of ex-
609 perimental tuour growth, *PLoS Comput. Biol.* 10 (8) (2014) e1003800.
- 610 [26] J. Chen, W. Sun, H. Zhang, J. Ma, P. Xu, Y. Yu, H. Fang, L. Zhou, J. Lv,
611 J. Xie, Y. Liu, K. Tang, B. Huang, Macrophages reprogrammed by lung
612 cancer microparticles promote tumour development via release of IL-1 β ,
613 *Cell. Mol. Immunol.* (2019) 1–12.
- 614 [27] A. A. Patel, Y. Zhang, J. N. Fullerton, L. Boelen, A. Rongvaux, A. A.
615 Maini, V. Bigley, R. A. Flavell, D. W. Gilroy, B. Asquith, et al., The
616 fate and lifespan of human monocyte subsets in steady state and systemic
617 inflammation, *Journal of Experimental Medicine* 214 (7) (2017) 1913–1923.
- 618 [28] E. Soucie, Z. Weng, L. Geirsdóttir, K. Molawi, J. Maurizio, R. Fenouil,
619 N. Mossadegh-Keller, G. Gimenez, L. VanHille, M. Beniazza, J. favret,
620 C. berruyer, P. Perrin, N. Hacoheh, J. Andrau, P. Ferrier, P. Dubreuil,
621 A. Sidow, M. Sieweke, Lineage-specific enhancers activate self-renewal
622 genes in macrophages and embryonic stem cells, *Science* 351 (6274) (2016)
623 aad5510.
- 624 [29] A. Poh, M. Ernst, Targeting macrophages in cancer: from bench to bedside,
625 *Frontiers in Oncology* 8 (2018) 49.
- 626 [30] V. Chitu, Y.-G. Yeung, W. Yu, S. Nandl, E. Stanley, Measurement of
627 macrophage growth and differentiation, *Curr. Protoc. Immunol.* (2011) 1–
628 26.
- 629 [31] P. Italiani, D. Boraschi, From monocytes to M1/M2 macrophages: phe-
630 notypical vs. functional differentiation, *Frontiers in Immunology* 5 (2014)
631 47–68.
- 632 [32] M. Heusinkveld, S. van der Burg, Identification and manipulation of tu-
633 mour associated macrophages in human cancers, *Journal of Translational
634 Medicine* 9 (2011) 216.
- 635 [33] T. Sato, M. Morita, R. Tanaka, Y. Inoue, M. Nomura, Y. Sakamoto,
636 K. Miura, S. Ito, I. Sato, N. Tanaka, J. Abe, S. Takahashi, M. Kawai,
637 M. Sato, Y. Hippo, H. Shima, Y. Okada, N. Tanuma, *Ex vivo* model of
638 non-small cell lung cancer using mouse lung epithelial cells, *Oncology Let-
639 ters* 14 (2017) 6863–6868.
- 640 [34] H. Yamaji, T. Iizasa, E. Koh, M. Suzuki, M. Otsuji, H. Chang, S. Mo-
641 tohashi, S. Yokoi, K. Hiroshima, M. Tagawa, T. Nakayama, T. Fujisawa,
642 Correlation between interleukin 6 production and tumour proliferation in
643 non-small cell lung cancer, *Cancer Immunol. Immunother.* 53 (786-792).

- 644 [35] P. Haley, B. Muggenburg, D. Weissman, D. Bice, Comparative morphology
645 and morphometry of alveolar macrophages from size mammalian species,
646 *American Journal of Anatomy* 4 (1991) 401–407.
- 647 [36] U. D. Monte, Does the cell number 10^9 still really fit one gram of tumour
648 tissue?, *Cell Cycle* 8 (3) (2009) 505–506.
- 649 [37] E. Redente, D. Orlicky, R. Bouchard, A. Malkinson, Tumour signalling
650 to the bone marrow changes the phenotype of monocytes and pulmonary
651 macrophages during urethane-induced primary lung tumorigenesis in a/j
652 mice, *Am. J. Pathol.* 170 (2007) 693–708.
- 653 [38] Z. Zi, Sensitivity analysis approaches applied to system biology models,
654 *IET Syst. Biol.* 5 (6) (2011) 336–346.
- 655 [39] J. Kirch, C. Tomaseth, A. Jensch, N. Radde, The effect of model rescaling
656 and normalization on sensitivity analysis on an example of a MAPK pathway
657 model, *EPJ Nonlinear Biomedical Physics* 4 (2016) 3.
- 658 [40] S. M. Blower, H. Dowlatabadi, Sensitivity and uncertainty analysis of com-
659 plex models of disease transmission: an HIV model, as an example, *Inter-
660 national Statistical Review* 62 (2) (1994) 229–243.
- 661 [41] S. Marino, I. B. Hogue, C. J. Ray, D. E. Kirschner, A methodology for
662 performing global uncertainty and sensitivity analysis in systems biology,
663 *Journal of Theoretical Biology* 254 (1) (2008) 178–196.
- 664 [42] D. Joseph, H. Bax, S. Karagiannis, Tumour-associated macrophage po-
665 larisation and re-education with immunotherapy, *Frontiers in Bioscience* 7
666 (2015) 334–351.
- 667 [43] A. Mantovani, F. Marchesi, A. Malesci, L. Laghi, P. Allavena, Tumour-
668 associated macrophages as treatment targets in oncology, *Nat. Rev. Clin.
669 Oncol.* 14 (7) (2017) 399–416.
- 670 [44] R. D. Boer, A. Perelson, Quantifying T lymphocyte turnover, *J. Theor.
671 Biol.* 327 (2013) 45–87.
- 672 [45] D. Macallan, R. Busch, B. Asquith, Current estimates of T cell kinetics in
673 humans, *Current Opinion in Systems Biology* 18 (2019) 77–86.